PNAS RESEARCH ARTICLE | PLANT BIOLOGY

Cotranscriptional splicing is required in the cold to produce *COOLAIR* isoforms that repress *Arabidopsis FLC*

Xiaogang Long[a,b,1], Yajun Cai[a,b,1], Huamei Wang[a], Yue Liu[a,b], Xiaoyi Huang[a,b], Hua Xuan[a,b], Wenjuan Li[a,b], Xiaoling Zhang[a,b], Hongya Zhang[a,b], Xiaofeng Fang[c,2], Hang He[d], Guoyong Xu[b,e], Caroline Dean[c,3], and Hongchun Yang[a,b,f,3]

Affiliations are included on p. 8.

Contributed by Caroline Dean; received April 16, 2024; accepted October 4, 2024; reviewed by Maria Carmo-Fonseca and Naeem Syed

Plants use seasonal cold to time the transition to reproductive development. Short- and long-term cold exposure is registered via parallel transcriptional shutdown and Polycomb-dependent epigenetic silencing of the *Arabidopsis thaliana* major flowering repressor locus *FLOWERING LOCUS C* (*FLC*). The cold-induced antisense transcripts (*COOLAIR*) determine the dynamics of *FLC* transcriptional shutdown, but the thermosensory mechanisms are still unresolved. Here, through a forward genetic screen, we identify a mutation that perturbs cold-induced *COOLAIR* expression and *FLC* repression. The mutation is a hypomorphic allele of SUPPRESSORS OF MEC-8 AND UNC-52 1 (SMU1), a conserved subunit of the spliceosomal B complex. SMU1 interacts in vivo with the proximal region of nascent *COOLAIR* and RNA 3′ processing/cotranscriptional regulators and enhances *COOLAIR* proximal intron splicing to promote specific *COOLAIR* isoforms. SMU1 also interacts with ELF7, an RNA Polymerase II Associated Factor (Paf1) component and limits *COOLAIR* transcription. Cold thus changes cotranscriptional splicing/RNA Pol II functionality in an SMU1-dependent mechanism to promote two different isoforms of *COOLAIR* that lead to reduced *FLC* transcription. Such cotranscriptional mechanisms are emerging as important regulators underlying plasticity in gene expression.

SMU1 | *COOLAIR* | *FLC* | cotranscription RNA splicing and processing | cold perception

Significance

How the environment modulates the genotype–phenotype interaction is a central question in the gene regulation field. We study how cold-induced antisense transcripts (*COOLAIR*) mediate transcriptional repression of *FLOWERING LOCUS C* (*FLC*) to promote flowering in *Arabidopsis*. Which aspects of cold regulation of *COOLAIR* are important to repress *FLC* transcription are still unclear. Here, we use a mutant screen to identify a role for SUPPRESSORS OF MEC-8 AND UNC-52 1 (SMU1), a core spliceosome protein, in linking cold exposure with changes in *COOLAIR* that influence *FLC* repression. Cold exposure promotes the production of two *COOLAIR* isoforms previously shown to repress *FLC* through two different mechanisms. *COOLAIR* cotranscriptional processing is thus part of a SMU-dependent, thermosensory mechanism repressing *FLC*.

Successful reproduction of angiosperms relies on careful timing of flowering to match favorable seasons. Temperature is one of the critical environmental factors that plants use to regulate flowering time. In *Arabidopsis thaliana*, a requirement for prolonged cold exposure aligns flowering to spring through a process called vernalization. This involves cold-dependent pathways that suppress the expression of the major floral repressor locus *FLOWERING LOCUS C* (*FLC*) (1–5). Antisense transcripts expressed from the 3′-end of the *FLC* locus, collectively called *COOLAIR*, are rapidly induced by cold and correlate with fast *FLC* transcriptional down-regulation (2, 6, 7). In parallel, a slower cold-induced Polycomb Repressive Complex 2 (PRC2) silencing mechanism generates an epigenetically silenced state (1, 8–11). These interconnected repression mechanisms efficiently silence *FLC* during cold, promoting the floral transition once plants return to warm temperatures.

COOLAIR expression is rapidly and transiently induced by cold, with more cells expressing higher levels within hours, lasting for 1 to 2 wk of cold exposure and forming dynamic nuclear foci (12). The two largest foci colocalize with the *FLC* locus, mirroring the situation with the noncoding RNA Xist clustered over the inactive mammalian X chromosome (13, 14). Sense and antisense transcription were shown to be mutually exclusive at each allele providing a mechanism by which *COOLAIR* represses *FLC* transcription in the cold (12). Disruption of *COOLAIR* transcription by insertions or deletions at its promoter, in most cases but not all, disrupts effective *FLC* repression (6, 7, 11). The parallel activities of the antisense-mediated transcriptional *FLC* repression, capable of fast response, and a slow PRC2 epigenetic silencing, means the pathways contribute differently in different conditions, with the antisense contribution to *FLC* silencing being particularly important in fluctuating temperatures (15).

Multiple isoforms of *COOLAIR* are formed through alternative splicing and polyadenylation. For example, a proximally polyadenylated isoform class I.i, a distal isoform class II.i and a cold-induced distal isoform class II.ii (Fig. 1*A*) (2). These isoforms differentially influence *FLC* chromatin state and transcriptional output (6, 16–19). The proximal class I.i isoform represses *FLC* transcription through activities of the RNA binding proteins FPA and FCA, core 3′ processing factors, pTEFb components, and histone H3 lysine 4 di/mono-methylation (H3K4me2/me1) modifiers FLOWERING LOCUS D (FLD),

Reviewers: M.C.-F., Universidade de Lisboa; and N.S., Canterbury Christ Church University.

The authors declare no competing interest.

[1]X.L. and Y.C. contributed equally to this work.

[2]Present address: Center for Plant Biology, School of Life Sciences, Tsinghua University, Beijing 100084, China.

[3]To whom correspondence may be addressed. Email: caroline.dean@jic.ac.uk or h.yang@whu.edu.cn.

This article contains supporting information online at https://www.pnas.org/lookup/suppl/doi:10.1073/pnas.2407628121/-/DCSupplemental.

Published November 15, 2024.

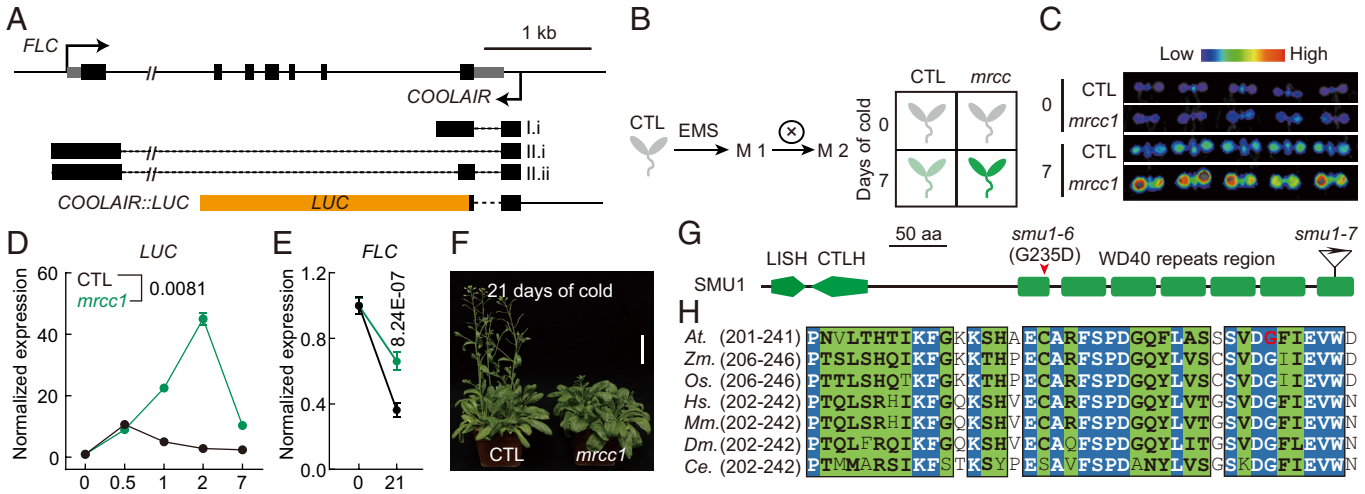

Fig. 1. The conserved splicing factor SMU1 is required for *COOLAIR* regulation and effective *FLC* repression in the cold. (*A*) Schematic comparison of the *COOLAIR::LUC* construct with *FLC* and *COOLAIR* transcripts at the *FLC* locus. *LUCIFERASE* is fused with part of the proximal *COOLAIR* sequence. Black arrows, transcriptional start sites (TSSs) and directions; gray boxes, untranslated regions; black boxes, exons; black lines, introns and intergenic regions of sense *FLC*; dashed lines, introns of *COOLAIR*. (*B*) Schematic picture showing the screening strategy. The progenitor line CTL was mutagenized by EMS and self-fertilized. LUC signal is measured for each M2 line before and after 7 d of cold treatment and compared with CTL plants. (*C*) *mrcc1* showing increased LUC signal from *COOLAIR::LUC* transgene after 7 d of cold treatment. (*D*) The expression levels of *LUC* normalized to nontreated levels in a time course of cold treatments assayed by RT-qPCR. The *X*-axis indicates the days of cold treatment. Data are presented as mean ± SD (n = 3). Significant difference is determined by paired two-tailed Student's *t* tests. (*E*) *FLC* expression levels before and after 21 d of cold treatment in CTL and *mrcc1*, with cold treatment normalized to nontreated *FLC* levels. The *X*-axis indicates the days of cold treatment. Error bars represent SD from six biological replicates. Significant difference is determined by unpaired two-tailed Student's *t* tests. (*F*) Flowering time of CTL and *mrcc1* plants after 21 d of cold treatment. The plants were imaged after transferring to the soil for 41 d. (Scale bar, 4 cm.) (*G*) Schematic picture showing the conserved domains of SMU1. The *mrcc1* mutation is located at the first WD40 domain and pointed by the red arrow, which changes a glycine (*G*) to aspartate (*D*) at amino acid position 235. The T-DNA insertion site and direction of *smu1-7* are displayed. (*H*) Alignment of the first WD40 domain of SMU1 containing the G235D mutation in *mrcc1*. The mutation site in *mrcc1* is indicated by a red letter. Blue background indicates the completely consistent amino acids; black box represents greater than or equal to 70% consistency in all species. *At*, *Arabidopsis thaliana* (NP_177513.2); *Zm*, *Zea mays* (NP_001167711.1); *Os*, *Oryza sativa* (XP_015621621.1); *Hs*, *Homo sapiens* (NP_060695.2); *Mm*, *Mus musculus* (NP_067510.3); *Dm*, *Drosophila melanogaster* (NP_001247189.1); *Ce*, *Caenorhabditis elegans* (NP_493279.1).

LUMINIDEPENDENS (LD), and SET DOMAIN GROUP 26 (SDG26) (20–24). These factors promote the formation of proximal *COOLAIR* class I.i, which leads to H3K4 demethylation in the *FLC* gene body and repression of *FLC* transcription (20).

The distal *COOLAIR* class II.ii isoform, induced by cold, shares the same first intron as class I.i but contains an extra exon compared to class II.i (2, 6). *COOLAIR* class II.ii interacts with FRIGIDA (FRI), a strong *FLC* activator, and sequesters FRI away from the *FLC* promoter, repressing *FLC* transcription (5, 6, 25, 26). Thus, *COOLAIR* isoforms play multiple and complex roles in *FLC* repression in the cold. *COOLAIR* expression is promoted by CRT/DRE-BINDING FACTORs (CBFs) in the cold (27), but knowledge of what aspects of cold regulation of *COOLAIR* and how it determines *FLC* down-regulation is still limited (27–29). We therefore undertook a forward genetic screen to identify other thermosensory steps. Here, we identify a hypomorphic allele of SUPPRESSORS OF MEC-8 AND UNC-52 1 (SMU1), a conserved subunit of the spliceosomal B complex that disrupts cold-induced *COOLAIR* up-regulation and function. Our findings show how cotranscriptional processing of long noncoding antisense RNAs contributes to the thermosensory mechanism registering short cold exposure.

Results

Screen for Mutants That Specifically Perturb *COOLAIR* Expression after Cold Exposure. To explore the cold-dependent regulation and function of *COOLAIR*, we screened for mutations that altered *COOLAIR* expression in the cold (Fig. 1 *A* and *B*) using a *COOLAIR::LUC* transgene: the *COOLAIR* promoter, first exon, proximal intron, and part of exon two, fused to *LUCIFERASE* (*LUC*) with a NOS 3′ terminator (Fig. 1*A*) (2, 11, 30). The *COOLAIR::LUC* was introduced into wild-type plants (WT, Col-*FRI*^{sf2}) and a single copy, homozygous progenitor line generated (CTL, *COOLAIR::LUC/FRI*^{sf2}), which was subjected to ethyl methane sulfonate (EMS) mutagenesis (Fig. 1 *A* and *B*). A mutant *Mis-Regulated COOLAIR in Cold 1* (*mrcc1*) was identified in which the LUC signal was the same as the wild-type (CTL) plants without cold but specifically enhanced in the cold (Fig. 1*C*). Consistently, the *LUC* RNA level was increased after short cold exposure (1 and 2 d of cold) (Fig. 1*D*). The cold-responsive factors CBFs stimulate *COOLAIR* expression by binding to the CRT/DRE cis-motif at the *COOLAIR* promoter after very short cold exposure (27, 31, 32), so we asked whether the mutation affected their expression. *CBF1*, *CBF2*, and *CBF3* displayed similar induction comparing *mrcc1* to CTL by 0.5 d of cold and then declined with slightly different dynamics; *CBF1* declined faster and *CBF2* and *CBF3* were similar (*SI Appendix*, Fig. S1). The expression dynamics of *CBFs* and *COOLAIR::LUC* suggested that the disrupted *COOLAIR::LUC* expression in *mrcc1* is unlikely to involve CBF regulation. We also measured the expression levels of *FLC* in *mrcc1* before and during the cold. *FLC* was not as effectively repressed by cold in the *mrcc1* plants as compared to wild type, a result further supported by the late flowering phenotype of the plants after cold treatment (Fig. 1 *E* and *F*). Hence, we had identified a mutation that enhanced *COOLAIR::LUC* expression and attenuated effective *FLC* repression in the cold.

To map the causal mutation of *mrcc1*, we backcrossed *mrcc1* with CTL. The BC1 F1 plants displayed a CTL-like LUC signal, with BC1 F2 plants segregating in a ratio of ~3:1 (low to high LUC), suggesting *mrcc1* is a single recessive mutation (*SI Appendix*, Fig. S2 *A* and *B*). The mutation was mapped to a ~4 M region on chromosome 1 by MutMap (33), containing eight candidate genes, seven protein-coding, and one noncoding gene (*SI Appendix*, Fig. S2 *C* and *D* and Dataset S1). We cloned the genomic sequence of each candidate gene and transformed them individually into

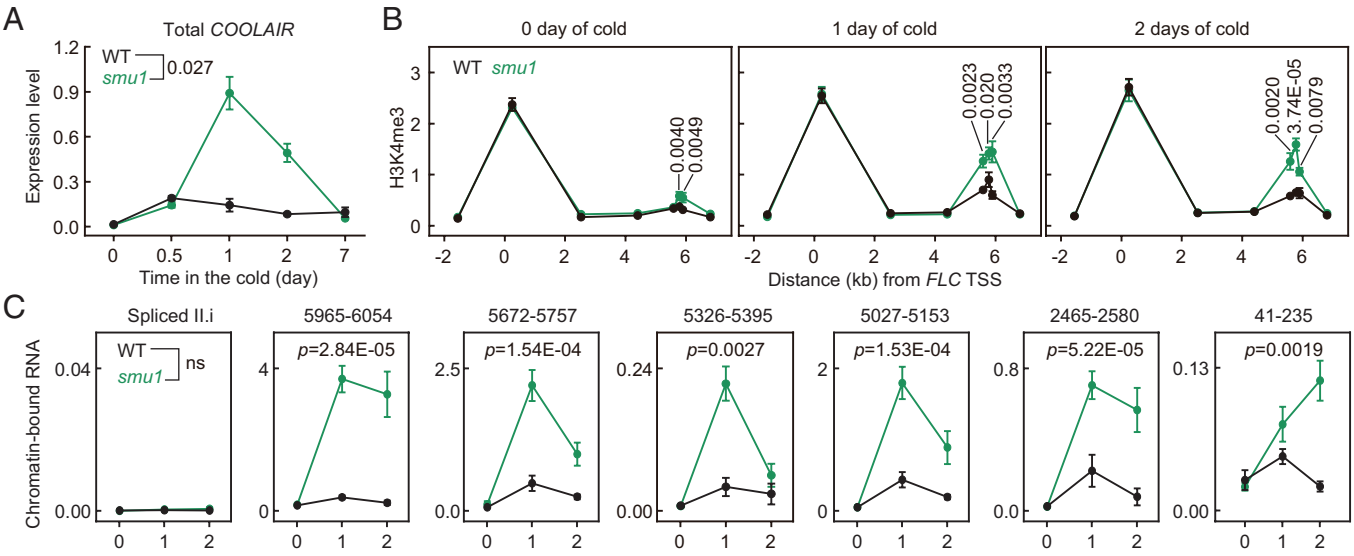

Fig. 2. SMU1 limits *COOLAIR* chromatin-bound RNA in the cold. (*A*) Expression levels assayed by RT-qPCR of total *COOLAIR* transcripts over a time course of cold treatment. Data are presented as mean ± SD (n = 3). Significant differences are determined by paired two-tailed Student's *t* tests. (*B*) H3K4me3 enrichment at *FLC* chromatin assayed by ChIP-qPCR. Data are presented as mean ± SEM (n = 6). A significant difference is determined by unpaired two-tailed Student's *t* tests. All the unlabeled points indicate no significant difference between WT and *smu1*. (*C*) Nascent transcript levels of *COOLAIR* measured by the levels of chromatin-bound RNA. The *X*-axis indicates the days of cold treatment. The assayed transcripts (relative position from *FLC* TSS) are indicated at the *Top*. The spliced class II.i was used as the control. Data are presented as mean ± SD (n = 6). Significant differences are determined by paired two-tailed Student's *t* tests (ns, no significant difference).

mrcc1. Only *SUPPRESSORS OF MEC-8 AND UNC-52 1* (*SMU1*, AT1G73720) complemented the *mrcc1* enhanced LUC signal, returning it to the CTL level in the T1 generation in the cold (*SI Appendix*, Fig. S2*D*). The complementation was further confirmed in homozygous plants in the T3 generation (*SI Appendix*, Fig. S2*E*). SMU1 is a conserved component of the spliceosomal B complex, bridging the U2 and U5 snRNPs and the dimerization of spliceosomal B complex, required for the 3′-splice site selection and processing of an intron (34–38). The mutation in *mrcc1* substituted a conserved glycine to aspartate at amino acid 235 (G235D) in the first WD40 repeat domain (Fig. 1 *G* and *H* and *SI Appendix*, Fig. S2*F*). Identification of the correct gene was confirmed by allelic analysis, through an *mrcc1* cross to heterozygous plants of *smu1-7* (embryo lethal as homozygote) (Fig. 1*G* and *SI Appendix*, Fig. S2*G*) (34). Approximately half of the F1 offspring was the heteroallelic combination of *smu1-7* and *mrcc1*. These plants exhibited *mrcc1*-like LUC activity; the *mrcc1*/WT heterozygous plants showed a CTL-like LUC activity (*SI Appendix*, Fig. S2*G*). Thus, we had cloned a hypomorphic mutation of *SMU1*.

To understand the cold-specific defect caused by the mutation of *SMU1* in *mrcc1*, we first measured the RNA expression dynamics of *SMU1* and found that these were not obviously altered by cold in either the wild-type or mutant (*SI Appendix*, Fig. S3*A*). We also made a *SMU1*^{G235D}*-GFP* transgenic line; mRNA levels of *SMU1-GFP* and *SMU1*^{G235D}*-GFP* were comparable but the SMU1^{G235D}-GFP protein level was much lower than that of SMU1-GFP both in NV and cold conditions (*SI Appendix*, Fig. S3 *B* and *C*). Thus, the defects caused by the missense mutation in *mrcc1* appear to be due to reduced protein level of *SMU1*.

SMU1 Limits *COOLAIR* Transcription after Cold Exposure. To explore the function of SMU1 on *COOLAIR* regulation, *mrcc1* was backcrossed into wild-type plants. The plants carrying the mutation but lacking the *COOLAIR::LUC* transgene were identified and named *smu1-6* (referred to as *smu1* without specification) (Fig. 1*G*). Total *COOLAIR*, and the unspliced transcript over the proximal and distal regions, increased in *smu1* after cold exposure (Fig. 2*A* and *SI Appendix*, Fig. S4). H3K4me3 over the proximal *COOLAIR* chromatin region has been found to correlate well with transcription (39). Chromatin immunoprecipitation (ChIP) showed that H3K4me3 enrichment increased in the cold in WT and further increased in *smu1* over this region (Fig. 2*B*). Analysis of chromatin-bound RNA, which includes the nascent transcript produced by transcribing RNA polymerase II (Pol II) also showed increased level of *COOLAIR* across the whole locus in *smu1* in the cold (Fig. 2*C*). We then sought to determine the level of RNA Pol II over *COOLAIR*. However, the convergent transcription of *COOLAIR* and *FLC* makes it hard to selectively assay Pol II only transcribing the *COOLAIR* strand. Since the *COOLAIR::LUC* transgene reflects endogenous *COOLAIR* transcription very well (*SI Appendix*, Fig. S5 *A* and *B*), we measured Pol II occupation over the *COOLAIR::LUC* transgene locus. Total Pol II and Ser2 phosphorylated Pol II were increased by cold in CTL and were even higher in *mrcc1* (*SI Appendix*, Fig. S5*C*). Thus, SMU1 appears to particularly affect *COOLAIR* transcription in the cold.

We identified EARLY FLOWERING 7 (ELF7) as an interactor of SMU1 in a yeast two-hybrid (Y2H) assay (Fig. 3 *A* and *B*). ELF7 is a conserved component of the Polymerase Associated Factor 1 (Paf1) complex, which interacts with Pol II and plays a role in effective transcription initiation and elongation (40–44). We found the LISH and CTLH domains at the SMU1 N-terminal and the Paf1 domain at the ELF7 C-terminal were necessary and sufficient for the interaction in yeast cells (Fig. 3 *A* and *B*), agreeing with the N-terminal of SMU1 serving as a scaffold for protein–protein interaction (35, 37). The interaction was further supported by a split firefly luciferase complementation (SFLC) assay and co-immunoprecipitation assays (Co-IP) after *Nicotiana benthamiana* (*N. ben*) transient transfection (*SI Appendix*, Fig. S6). To test whether ELF7 interacts with SMU1 in *Arabidopsis*, a transgenic line carrying a translational SMU1-GFP fusion was generated that fully complemented the transcription defects of *smu1* on *COOLAIR* (*SI Appendix*, Fig. S7 *A* and *B*). SMU1-GFP localized to the nucleus and was enriched by immunoprecipitation (*SI Appendix*, Fig. S7 *C* and *D*). A *FLAG-ELF7/elf7* line (45) was crossed with *SMU1-GFP/smu1* plants and the seedlings carrying both *FLAG-ELF7* and *SMU1-GFP* were subjected to Co-IP.

FLAG-ELF7 and SMU1-GFP coprecipitated after formaldehyde cross-linking (Fig. 3*C*) but not in non-cross-linked plants, suggesting ELF7 transiently associates with SMU1 in vivo. Increased FLAG-ELF7 was immunoprecipitated with SMU1-GFP from the cold exposed plants, suggesting a stronger or more abundant interaction (Fig. 3*C*). Furthermore, ELF7 occupancy was elevated at *FLC* chromatin in *smu1* after cold (Fig. 3*D*). Next, we analyzed the genetic interaction between SMU1 and ELF7 in *COOLAIR* regulation. The expression level of *COOLAIR* was reduced in *elf7* in warm-grown (NV) and cold-treated plants (Fig. 3*E*); thus, ELF7 is required for the productive expression of *COOLAIR*. The *smu1* mutation-induced ectopic expression of *COOLAIR* in the cold was diminished in *elf7 smu1*; *COOLAIR* expression was similar in *elf7* and *elf7 smu1* (Fig. 3*E*). These data support the view that SMU1 affects *COOLAIR* transcription through an influence on ELF7 function in the cold.

SMU1 Binds Nascent Transcripts to Promote the Processing of Proximal *COOLAIR*. As SMU1 is a conserved component of the spliceosomal B complex, we used the *SMU1-GFP/smu1* transgenic line to test whether SMU1 associates with *COOLAIR* RNA. RNA-immunoprecipitation (RIP) showed that SMU1 was specifically enriched at the proximal region of unspliced *COOLAIR* (Fig. 4*A*); this enrichment was further stimulated by cold, not due to the increased *COOLAIR* RNA level and SMU1 expression (Fig. 4*A* and *SI Appendix*, Fig. S7 *E* and *F*). We also found that SMU1 did not associate with the distal region or spliced proximal *COOLAIR* (class I.i) (Fig. 4*A*). Thus, SMU1 associates with the proximal region of nascent *COOLAIR* transcripts.

The spliceosomal B complex is essential in cotranscriptional splicing (34–38) and SMU1 associates with nascent proximal *COOLAIR*. We, therefore, performed a detailed analysis of *COOLAIR* splicing in the cold. Unexpectedly, levels of the spliced proximal class I.i decreased, while the spliced distal isoform (class II.i) levels increased in *smu1* in the cold (Fig. 4 *B* and *C*). The observation suggested that SMU1 plays distinct roles in splicing different *COOLAIR* isoforms. We thus analyzed splicing of both isoforms through the ratio of spliced to unspliced and found that the ratio for class II.i in *smu1* was similar to or higher than WT, before and in cold conditions (Fig. 4*D*). However, the ratio for the proximal intron (contained in class I.i) was significantly reduced in the cold in *smu1* (Fig. 4*E*). This defect was complemented by the *SMU1-GFP* transgene (*SI Appendix*, Fig. S7 *G* and *H*). Reduced efficiency of *COOLAIR* proximal intron splicing in *smu1* reduces production of class I.i (Fig. 4 *B* and *E*), an isoform linked to a silenced chromatin state at *FLC* (18, 20–23, 46–48).

The proteins that regulate class I.i transcription, splicing, 3′-end processing and polyadenylation dynamically interact in vivo (20, 46). One of these proteins, the RNA binding protein FPA (22, 49) enriched SMU1 and the central splicing regulator PRP8 after affinity purification following cross-linking (Fig. 4*F*). PRP8 represses *FLC* by promoting class I.i splicing (21). In addition, RNA binding proteins, FCA and FLOWERING LOCUS KH DOMAIN (FLK), 3′-end processing factors CLEAVAGE STIMULATING FACTOR 64 (CSTF64) and CSTF77, and Pol II regulators CDKC2 and GLOBAL TRANSCRIPTION FACTOR C (SPT16) were also enriched by FPA (Fig. 4*F* and Dataset S2). These had previously been shown to promote proximal *COOLAIR* processing to generate a silenced chromatin state that represses *FLC* expression (21–23). The association of SMU1 with FPA was further validated by additional Co-IP experiments (Fig. 4*G*).

In contrast to the effects on proximal *COOLAIR* intron splicing, the splicing efficiencies as judged by the ratio of spliced to unspliced transcript for *FLC* sense introns 1 and 5 were not changed in *smu1*, even though the intron lengths were similar to distal and proximal introns of *COOLAIR*, respectively (*SI Appendix*, Fig. S8). In summary, SMU1 associates with both the nascent *COOLAIR* transcripts and the protein factors known to promote proximal *COOLAIR* processing, thus specifically promoting the production of proximal *COOLAIR* (class I.i) and contributing to efficient *FLC* repression in the cold.

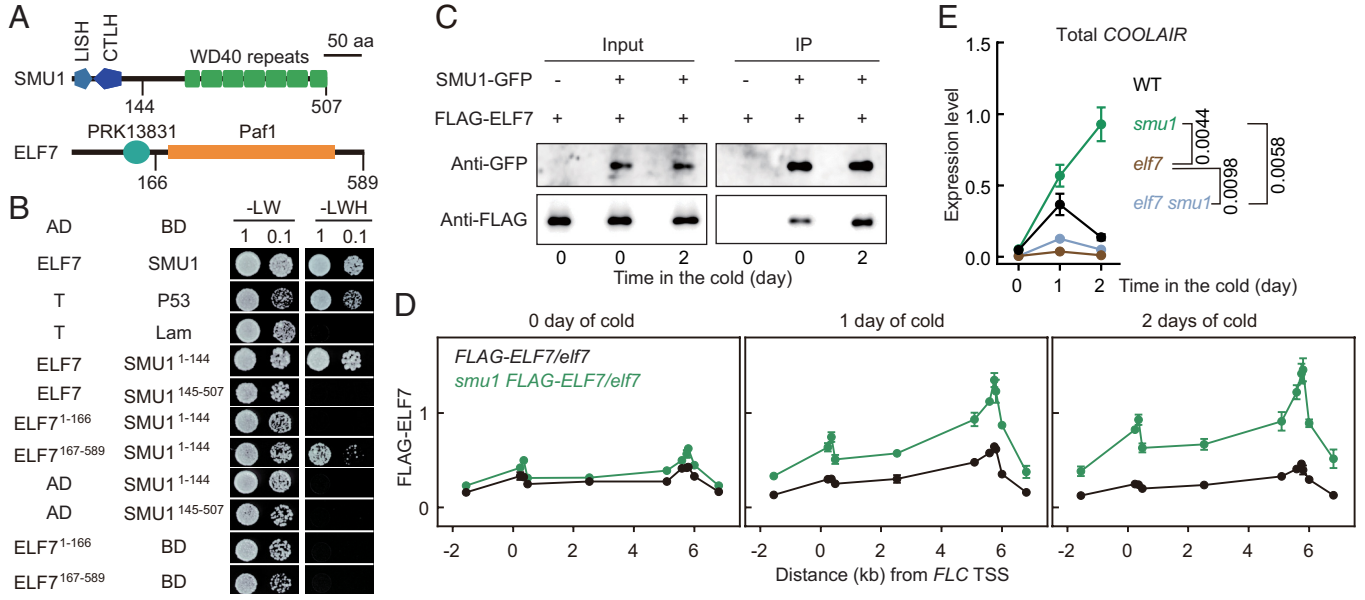

Fig. 3. SMU1 reduces ELF7 accumulation on *COOLAIR* chromatin in the cold. (*A*) Diagrams showing domains of SMU1 and ELF7. The numbers indicate the regions used in the Y2H assay. (*B*) SMU1 interacts with ELF7 in yeast cells. The pairs of indicated plasmids were cotransformed and grown on selective solid media lacking tryptophane (Trp, W), leucine (Leu, L), and histidine (His, H) (SD-WLH). T, SV40 large T-antigen; Lam, Lamin. (*C*) Co-IP of SMU1 and ELF7 before and after cold treatment in vivo. *FLAG-ELF7/elf7* served as a negative control. Samples before and after immunoprecipitation were detected by anti-FLAG and anti-GFP. (*D*) ELF7 enrichment at *FLC* in plants expressing FLAG-ELF7 assayed by ChIP-qPCR. Data are presented as mean ± SEM (n = 4). (*E*) Expression levels of total *COOLAIR* in WT, *smu1*, *elf7*, and *elf7 smu1* assayed by RT-qPCR. The seedlings of indicated genotypes are treated with 0, 1, and 2 d of cold. Data are presented as mean ± SD (n = 3), and significant differences are determined by paired two-tailed Student's *t* tests.

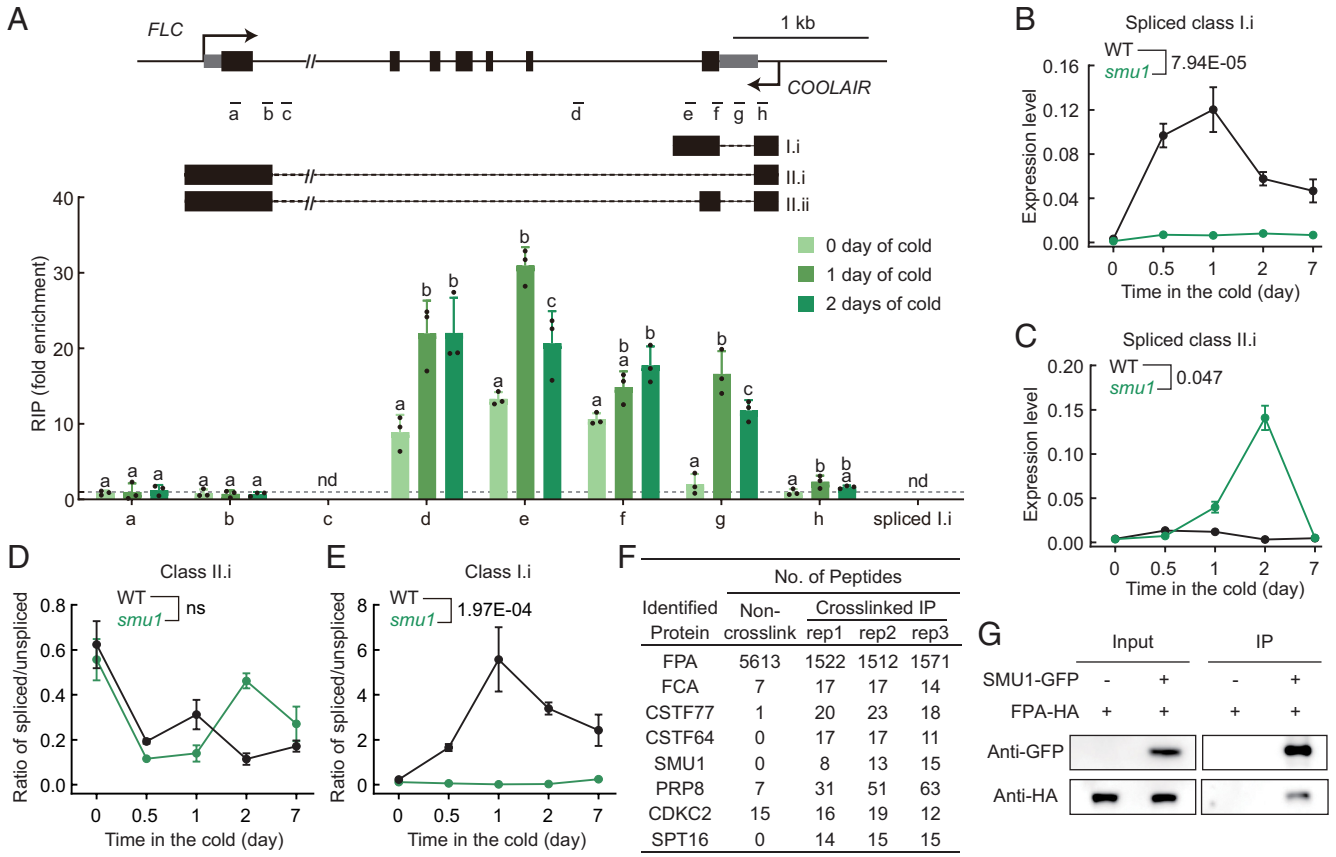

Fig. 4. SMU1 promotes proximal *COOLAIR* processing in the cold. (*A*) RIP analysis of SMU1 enrichment on *COOLAIR* using *SMU1-GFP/smu1 #7* complementation transgenic line. nd, not detected. The wild-type plant was used as the control, and the level at each fragment is set as "1" (indicated by the dashed gray line). The position of each detected region relative to *COOLAIR* transcripts is displayed. Data are presented as mean ± SD (n = 3). The lowercase letters indicate significant differences ($P < 0.05$) analyzed by one-way ANOVA of Sidak's multiple comparisons test between each tested region. (*B*) and (*C*) Expression levels of *COOLAIR* spliced class I.i (*B*) and spliced class II.i (*C*) assayed by RT-qPCR over a time course of cold treatment. Data are presented as mean ± SD (n = 3). (*D*) and (*E*) Splicing efficiencies of *COOLAIR* class II.i (*D*) and class I.i (*E*), as judged by the ratio of spliced to unspliced, in a time course of cold treatments assayed by RT-qPCR. Significant differences are determined by paired two-tailed Student's *t* tests (ns, no significant difference) in (*B–E*). (*F*) List of proteins identified by cross-linked affinity purification of FPA. (*G*) SMU1 interacts with FPA assayed by Co-IP in *Arabidopsis* protoplasts. Samples before and after immunoprecipitation were detected by anti-HA and anti-GFP.

Reduced Class II.ii of *COOLAIR* in *smu1* Leads to Decreased FRI Condensation in the Cold. Class II.ii of *COOLAIR* is specifically induced by cold and required for effective *FLC* repression in the cold (2, 6, 7). Since class II.ii shares the same proximal intron as class I.i (Fig. 1*A*), we measured the level of spliced class II.ii, and found like class I.i, the levels of class II.ii were also reduced in *smu1* in the cold (Fig. 5*A*). Class II.ii immunoprecipitates FRI in vivo after ~3 to 6 h of cold and sequesters FRI into nuclear condensates, which do not colocalize with the *FLC* locus, hence repressing *FLC* transcription (6, 29). This conclusion has recently been challenged (6, 28, 29). Since *smu1* disrupts the production of class II.ii in the cold (Fig. 5*A*), it provides excellent material to address this issue. We, therefore, crossed the *FRI-GFP* transgenic line with *smu1* to generate *smu1 FRI-GFP*. The *smu1* mutation did not alter FRI protein levels, which increased in the cold (*SI Appendix*, Fig. S9) (6). Consistent with our previous observations, cold promotes FRI-GFP to form nuclear condensates, increasing condensate number and size (Fig. 5 *B–F*) (6, 28, 29). The condensates were reduced in size and number in *smu1* in the cold (Fig. 5 *B–F*). This supports the conclusion that *COOLAIR* class II.ii promotes FRI condensate formation and *FLC* repression in the cold.

SMU1-Mediated *FLC* Repression Functions through *COOLAIR* Proximal Intron Splicing. Because *COOLAIR* class I.i and II.ii are both involved in *FLC* repression (6, 18, 20–23, 46) and share the same proximal intron. We further investigated the function of proximal intron splicing in *FLC* repression in the cold. We first created an *FLC* deletion line (*flc-de*) by CRISPR/Cas9 genome editing to avoid any possible cross-effect from the endogenous locus (*SI Appendix*, Fig. S10 *A–D*). Second, in a transgene construct, we replaced the *COOLAIR* proximal intron–exon junction sequence from agGT to aaGT ($COOLAIR^{AA}$) (21) or aaAT- to remove the newly generated AG dinucleotide- ($COOLAIR^{AAA}$) to specifically inhibit the splicing of *COOLAIR* proximal intron, and the $COOLAIR^{WT}$ was used as the control (Fig. 6*A* and *SI Appendix*, Fig. S10 *A* and *B*). All three transgene constructs were transformed into the *flc-de* plants. All three transgenes displayed similar cold-induced *COOLAIR* expression but as expected, there was little spliced *COOLAIR* class I.i and II.ii in the $COOLAIR^{AA}$ and $COOLAIR^{AAA}$ transgenic lines, whereas spliced class II.i remained similar to $COOLAIR^{WT}$ (Fig. 6 *A–D* and *SI Appendix*, Fig. S10 *E–G*). This shows the mutation(s) specifically and effectively block *COOLAIR* proximal intron splicing (Fig. 6 *B–D* and *SI Appendix*, Fig. S10 *H* and *I*). *FLC* could not be effectively repressed in the $COOLAIR^{AA}$ and $COOLAIR^{AAA}$ transgenic lines compared to $COOLAIR^{WT}$ in the cold (Fig. 6*E*), supporting that splicing of *COOLAIR* proximal intron is indeed required for effective *FLC* repression in the cold.

Spliced class II.ii of *COOLAIR* promotes FRI sequestration away from the *FLC* promoter (6, 29). Since $COOLAIR^{AA}$ and $COOLAIR^{AAA}$ disrupt the production of spliced class II.ii (Fig. 6*D*), we tested FRI condensation in $COOLAIR^{AA}$ and $COOLAIR^{AAA}$ plants. FRI-GFP was crossed with the $COOLAIR^{WT}$/*flc-de*, $COOLAIR^{AA}$/*flc-de*, and

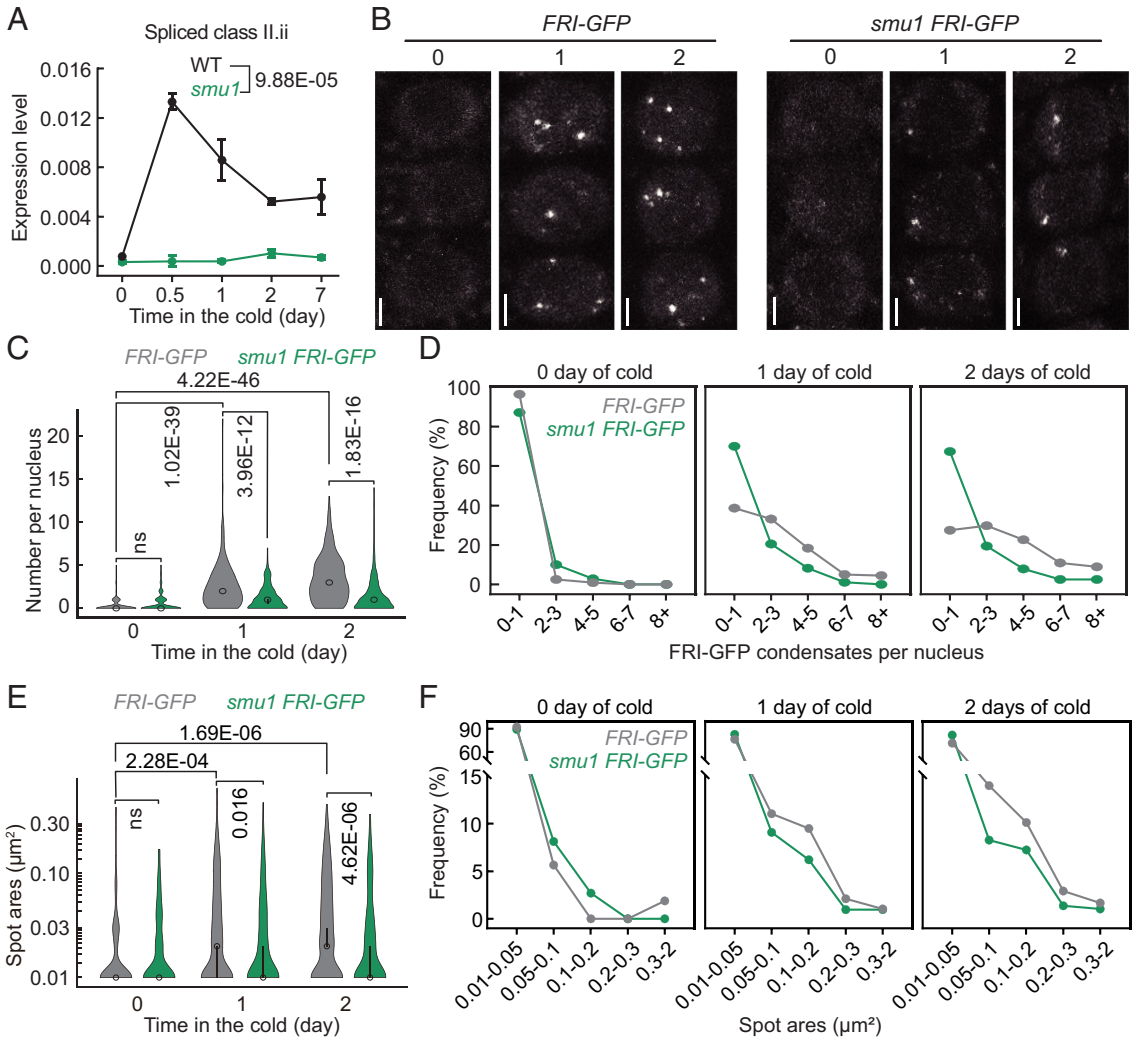

Fig. 5. SMU1 stimulates the production of class II.ii of *COOLAIR* and FRI sequestration in the condensates in the cold. (*A*) Expression levels of *COOLAIR* spliced class II.ii assayed by RT-qPCR over a time course of cold treatment. Data are presented as mean ± SD (n = 3). Significant differences are determined by paired two-tailed Student's *t* tests. (*B*) Comparing FRI-GFP condensates with or without *smu1* in root tip cells after 0, 1, and 2 d of cold treatment by confocal microscopic images. (Scale bar, 5 μm.) (*C*) Quantification of FRI-GFP condensates number per nucleus after 0, 1, and 2 d of cold treatments in the indicated genotypes. An open circle indicates the median of the data, and a vertical bar indicates the 95% CI determined by bootstrapping. Numbers of nuclei from numbers of plants (total nuclei/total plants) are (from *Left* to *Right*) 191/12, 201/13, 217/10, 180/10, 211/10, 190/12. Comparison of mean values is performed using the Mann–Whitney test (ns, no significant difference). (*D*) Frequency distribution of FRI-GFP condensates numbers per nucleus in root cells. (*E*) Quantification of the size of each FRI-GFP condensate in the indicated plants. An open circle indicates the median of the data, and a vertical bar indicates the 95% CI determined by bootstrapping. The numbers of analyzed condensates were (from *Left* to *Right*) 53, 111, 570, 209, 722, and 290. Comparison of mean values is performed using the Mann–Whitney test (ns, no significant difference). (*F*) Frequency distribution of FRI-GFP condensates spot area in root cells.

COOLAIR^{AAA}*/flc-de*. We found that the number of FRI-GFP condensates was reduced in the root tip cells of the *FRI-GFP COOLAIR*^{AA}*/flc-de* and *FRI-GFP COOLAIR*^{AAA}*/flc-de* seedlings when compared to the *FRI-GFP COOLAIR*^{WT}*/flc-de* seedlings (Fig. 6 *F* and *G*). This observation again supported that spliced class II.ii promotes FRI condensation in the cold.

The defects of the proximal intron splicing of *COOLAIR*, ineffective *FLC* repression, and reduced FRI condensation in the *COOLAIR*^{AA} and *COOLAIR*^{AAA} transgenic lines phenocopied the *smu1* mutation. We, therefore, generated *smu1 COOLAIR*^{AA} and *smu1 COOLAIR*^{AAA} double mutants with *smu1 COOLAIR*^{WT} as the control to test whether the SMU1-mediated *FLC* repression is dependent on *COOLAIR* proximal intron splicing. First, we detected similar hyperactivation and disrupted proximal intron splicing of *COOLAIR* in *smu1 COOLAIR*^{WT} and *smu1*, indicating SMU1 functions on transgenic and endogenous *COOLAIR* (Fig. 6 *B–D* and *SI Appendix*, Fig. S10 *E–I*). Second, *smu1 COOLAIR*^{WT}, *smu1 COOLAIR*^{AA}, and *smu1 COOLAIR*^{AAA} displayed higher *COOLAIR* expression in the cold (Fig. 6 *B–D* and *SI Appendix*, Fig. S10 *E–G*). Then, we measured *FLC* expression levels and found that the *FLC* repression defects in the cold were similar among *COOLAIR*^{AA}, *COOLAIR*^{AAA}, *smu1 COOLAIR*^{AA}, and *smu1 COOLAIR*^{AAA} (Fig. 6*E*). These observations support the importance of SMU1-dependent *COOLAIR* proximal intron splicing promoting *FLC* repression.

Discussion

Molecular dissection of the mechanism of vernalization has identified two interconnecting pathways that repress the major flowering repressor locus *FLC* in *Arabidopsis*. One is *COOLAIR*-mediated cotranscriptional repression, which can respond quickly or slowly depending on conditions, and the second is a slow cold-induced PRC2 epigenetic silencing (15). However, still relatively little was understood about what aspects of the *COOLAIR* dynamics are required for *FLC* repression. Thus, we took a forward genetic approach using a *COOLAIR::LUC*

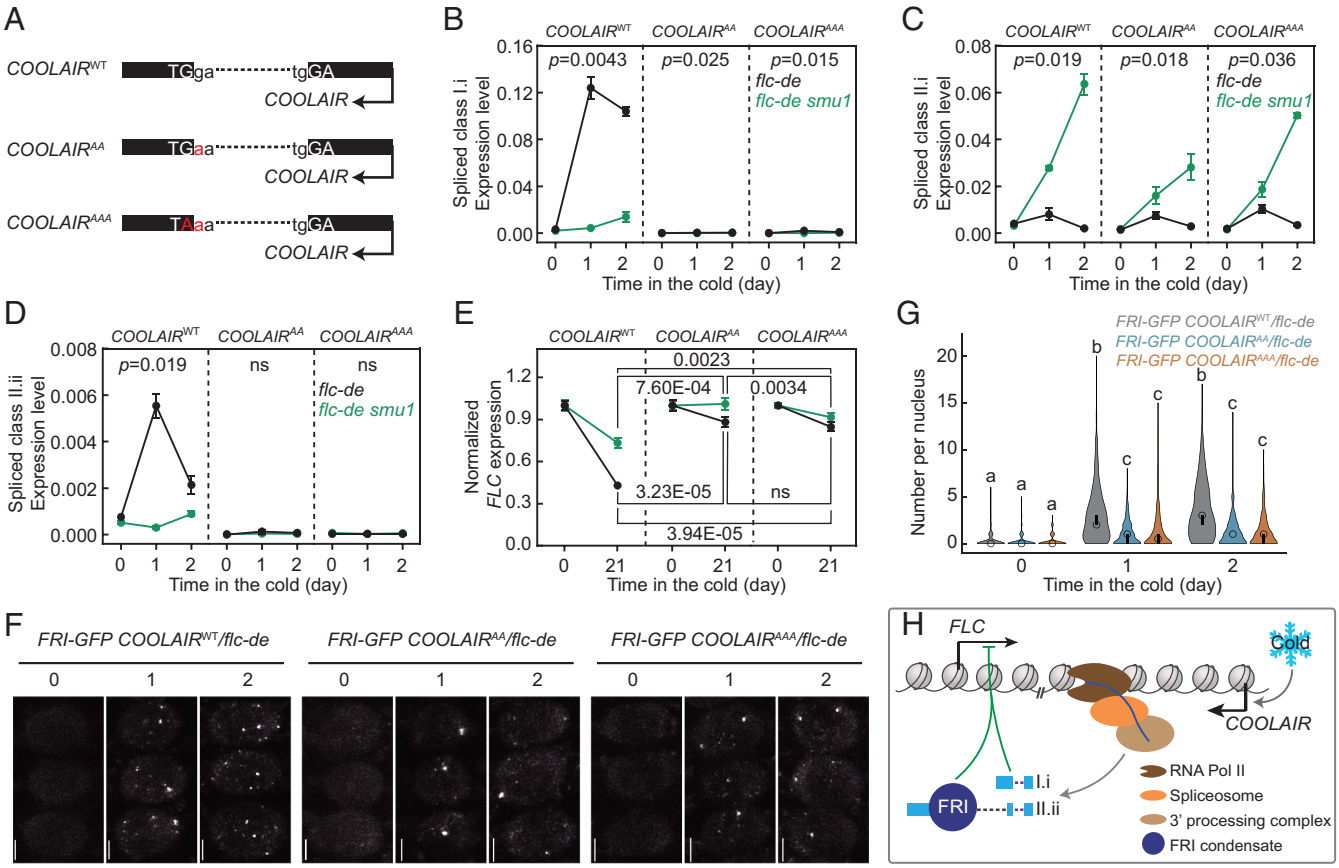

Fig. 6. SMU1-mediated *COOLAIR* proximal intron splicing promotes *FLC* repression in the cold. (*A*) Schematic representation of *COOLAIR* proximal intron–exon junction sequence in the *COOLAIR*^{WT} or at the mutated splice sites of *COOLAIR*^{AA} and *COOLAIR*^{AAA}. (*B–D*) Expression levels of spliced class I.i (*B*), spliced II.i (*C*), and spliced II.ii (*D*) of *COOLAIR* in *COOLAIR*^{WT}, *COOLAIR*^{AA}, and *COOLAIR*^{AAA} transgenic lines under *flc-de* and *flc-de smu1* backgrounds assayed by RT-qPCR. The seedlings of indicated genotypes are treated with 0, 1, and 2 d of cold. Data are presented as mean ± SD (n = 3), and significant differences are determined by paired two-tailed Student's *t* tests (ns, no significant difference). (*E*) *FLC* expression levels before and after 21 d of cold treatment in *COOLAIR*^{WT}, *COOLAIR*^{AA}, and *COOLAIR*^{AAA} transgenic lines under *flc-de* and *flc-de smu1* backgrounds assayed by RT-qPCR. The expression level without cold treatment is set as "1" in each genotype. Data are presented as mean ± SD (n = 3). Significant differences are determined by unpaired two-tailed Student's *t* tests (ns, no significant difference). (*F*) FRI-GFP condensates in root tip cells after 0, 1, and 2 d of cold treatment in *FRI-GFP COOLAIR*^{WT}*/flc-de*, *FRI-GFP COOLAIR*^{AA}*/flc-de*, and *FRI-GFP COOLAIR*^{AAA}*/flc-de* seedlings using confocal microscopy. (Scale bar, 5 μm.) (*G*) Quantification of FRI-GFP condensate number per nucleus after 0, 1, and 2 d of cold treatment in the indicated genotypes. An open circle indicates the median of the data, and a vertical bar indicates the 95% CI determined by bootstrapping. Numbers of nuclei from numbers of plants (total nuclei/total plants) are (from *Left* to *Right*) 199/10, 243/10, 218/9, 238/13, 239/10, 203/10, 205/13, 252/10, and 225/10. The different lowercase letters indicate significant differences ($P < 0.05$) analyzed by Mann–Whitney test. (*H*) A working model for SMU1 mediated cotranscriptional *COOLAIR* regulation in *FLC* repression in the cold.

reporter line to screen specifically for mutations that disrupt *COOLAIR* regulation in the cold (11, 30). This identified a hypomorphic mutation in the conserved spliceosome component SMU1 (Fig. 1 and *SI Appendix*, Fig. S2). We then investigated the mechanism at play. Altogether, our experiments describe a cotranscriptional splicing mechanism required in the cold to produce *COOLAIR* isoforms that repress *FLC* transcription (Fig. 6*H*), as one component of thermosensory inputs plants use to register winter.

SMU1 functions in a cotranscriptional mechanism that promotes splicing of the proximal *COOLAIR* intron and affects *COOLAIR* transcription as judged by chromatin-bound RNA, similar to other systems where alternative splicing is coupled with transcription and chromatin structure (50). H3K4me3 levels increased in the cold over the proximal region of *COOLAIR*, with the increase proportionately larger in *smu1*, with similar effects observed for ELF7 association with *FLC* chromatin (Figs. 2 and 3). Thus, SMU1 appears to function in a cotranscriptional mechanism influencing transcriptional output and impacting splice site choice, potentially by affecting RNA Pol II processivity/elongation. The final outcome in wild-type plants is the promotion of *COOLAIR* proximal intron splicing in the cold. This then represses *FLC* expression through two mechanisms: first, a class I.i-dependent transcription-termination coupled delivery of histone demethylation similar to that in warm conditions but involving other factors (18, 20, 22, 46–48, 51); second, sequestration of FRI by class II.ii into nuclear condensates away from the *FLC* promoter (6).

Such mechanisms linking chromatin regulation, transcription, and cotranscriptional splicing have been associated with environmental adaptation and stress response (52–54) and in *Arabidopsis* are important for response to environmental stimuli such as temperature and light (54, 55). A glycine to arginine substitution in the fifth WD40 domain of mammalian SMU1 results in temperature-sensitive cell cycle arrest (56, 57), so these cotranscriptional mechanisms may play a widespread role in gene expression plasticity.

Materials and Methods

Detailed information on plant material and growth conditions, mutagenesis, LUC signal assay, mutant mapping, allelism test, RNA expression analysis and RT-qPCR, ChIP and qPCR, preparation and quantification of chromatin-bound

RNA, yeast two-hybrid assay, SFLC assay, western blot and Co-IP, cross-linked nuclear immunoprecipitation and mass spectrometry, RIP and quantification, and microscopy is provided in *SI Appendix, Materials and Methods*.

Data, Materials, and Software Availability. Sequencing data for MutMap have been deposited in the China National Center for Bioinformation (CNCB) under accession number CRA013281 (58). All other data are included in the article and/or supporting information.

ACKNOWLEDGMENTS. We thank Qin Lu for equipment handling, Professor Ligeng Ma (Capital Normal University, China) for *FLAG-ELF7/elf7* and *elf7* seeds, Professor Liang Chen (Wuhan University, China) and Professor Kaiwei Liang (Wuhan University, China) for helpful assistance, and members of the C.D. and H.Y. research groups for discussions. H.Y. lab was supported by National Natural Science Foundation of China (32370619 and 31871301), Fundamental Research Funds for the Central Universities (2042022rc0007), the Natural Science Foundation of Hubei Province (2024AFA010), Hubei Hongshan Laboratory, and a start-up fund from Wuhan University. C.D. was supported by a Royal Society Professorship and Wellcome grant 210654.

Author affiliations: [a]State Key Laboratory of Hybrid Rice, College of Life Sciences, Wuhan University, Wuhan 430072, China; [b]Hubei Hongshan Laboratory, Wuhan 430070, China; [c]Cell and Developmental Biology, John Innes Centre, Norwich Research Park, Norwich NR4 7UH, United Kingdom; [d]College of Life Sciences, Peking University, Beijing 100871, China; [e]State Key Laboratory of Hybrid Rice, Institute for Advanced Studies, Wuhan University, Wuhan 430072, China; and [f]RNA Institute, Wuhan University, Wuhan 430072, China

Author contributions: X.L., H.W., H.H., G.X., C.D., and H.Y. designed research; X.L., Y.C., H.W., Y.L., X.H., H.X., W.L., X.Z., H.Z., X.F., and H.Y. performed research; X.L., Y.C., Y.L., H.H., C.D., and H.Y. analyzed data; and X.L., C.D., and H.Y. wrote the paper.

1. H. Yang *et al.*, Distinct phases of Polycomb silencing to hold epigenetic memory of cold in *Arabidopsis*. *Science* **357**, 1142–1145 (2017).
2. S. Swiezewski, F. Liu, A. Magusin, C. Dean, Cold-induced silencing by long antisense transcripts of an *Arabidopsis* Polycomb target. *Nature* **462**, 799–802 (2009).
3. S. D. Michaels, R. M. Amasino, *FLOWERING LOCUS C* encodes a novel MADS domain protein that acts as a repressor of flowering. *Plant Cell* **11**, 949–956 (1999).
4. J. Hepworth *et al.*, Absence of warmth permits epigenetic memory of winter in *Arabidopsis*. *Nat. Commun.* **9**, 639 (2018).
5. U. Johanson *et al.*, Molecular analysis of *FRIGIDA*, a major determinant of natural variation in *Arabidopsis* flowering time. *Science* **290**, 344–347 (2000).
6. P. Zhu, C. Lister, C. Dean, Cold-induced *Arabidopsis* FRIGIDA nuclear condensates for *FLC* repression. *Nature* **599**, 657–661 (2021).
7. T. Csorba, J. I. Questa, Q. Sun, C. Dean, Antisense *COOLAIR* mediates the coordinated switching of chromatin states at *FLC* during vernalization. *Proc. Natl. Acad. Sci. U.S.A.* **111**, 16160–16165 (2014).
8. F. De Lucia, P. Crevillen, A. M. Jones, T. Greb, C. Dean, A PHD-polycomb repressive complex 2 triggers the epigenetic silencing of *FLC* during vernalization. *Proc. Natl. Acad. Sci. U.S.A.* **105**, 16831–16836 (2008).
9. A. Angel, J. Song, C. Dean, M. Howard, A Polycomb-based switch underlying quantitative epigenetic memory. *Nature* **476**, 105–108 (2011).
10. S. Berry, M. Hartley, T. S. Olsson, C. Dean, M. Howard, Local chromatin environment of a Polycomb target gene instructs its own epigenetic inheritance. *Elife* **4**, e07205 (2015).
11. Y. Zhao *et al.*, Natural temperature fluctuations promote *COOLAIR* regulation of *FLC*. *Genes Dev.* **35**, 888–898 (2021).
12. S. Rosa, S. Duncan, C. Dean, Mutually exclusive sense–antisense transcription at *FLC* facilitates environmentally induced gene repression. *Nat. Commun.* **7**, 13031 (2016).
13. C. M. Clemson, J. A. McNeil, H. F. Willard, J. B. Lawrence, XIST RNA paints the inactive X chromosome at interphase: Evidence for a novel RNA involved in nuclear/chromosome structure. *J. Cell Biol.* **132**, 259–275 (1996).
14. J. M. Engreitz *et al.*, The Xist lncRNA exploits three-dimensional genome architecture to spread across the X chromosome. *Science* **341**, 1237973 (2013).
15. M. Nielsen *et al.*, *COOLAIR* and PRC2 function in parallel to silence *FLC* during vernalization. *Proc. Natl. Acad. Sci. U.S.A.* **121**, e2311474121 (2024).
16. M. Yang *et al.*, In vivo single-molecule analysis reveals *COOLAIR* RNA structural diversity. *Nature* **609**, 394–399 (2022).
17. P. Li, Z. Tao, C. Dean, Phenotypic evolution through variation in splicing of the noncoding RNA *COOLAIR*. *Genes Dev.* **29**, 696–701 (2015).
18. F. Liu *et al.*, The *Arabidopsis* RNA-binding protein FCA requires a lysine-specific demethylase 1 homolog to downregulate *FLC*. *Mol. Cell* **28**, 398–407 (2007).
19. Y. Tian *et al.*, PRC2 recruitment and H3K27me3 deposition at *FLC* require FCA binding of *COOLAIR*. *Sci. Adv.* **5**, eaau7246 (2019).
20. X. Fang *et al.*, The 3′ processing of antisense RNAs physically links to chromatin-based transcriptional control. *Proc. Natl. Acad. Sci. U.S.A.* **117**, 15316–15321 (2020).
21. S. Marquardt *et al.*, Functional consequences of splicing of the antisense transcript *COOLAIR* on *FLC* transcription. *Mol. Cell* **54**, 156–165 (2014).
22. F. Liu, S. Marquardt, C. Lister, S. Swiezewski, C. Dean, Targeted 3′ processing of antisense transcripts triggers *Arabidopsis FLC* chromatin silencing. *Science* **327**, 94–97 (2010).
23. Z. W. Wang, Z. Wu, O. Raitskin, Q. Sun, C. Dean, Antisense-mediated *FLC* transcriptional repression requires the P-TEFb transcription elongation factor. *Proc. Natl. Acad. Sci. U.S.A.* **111**, 7468–7473 (2014).
24. Z. Wu, X. Fang, D. Zhu, C. Dean, Autonomous pathway: *FLOWERING LOCUS C* repression through an antisense-mediated chromatin-silencing mechanism. *Plant Physiol.* **182**, 27–37 (2020).
25. K. Choi *et al.*, The FRIGIDA complex activates transcription of *FLC*, a strong flowering repressor in *Arabidopsis*, by recruiting chromatin modification factors. *Plant Cell* **23**, 289–303 (2011).
26. D. Jiang, X. Gu, Y. He, Establishment of the winter-annual growth habit via *FRIGIDA*-mediated histone methylation at *FLOWERING LOCUS C* in *Arabidopsis*. *Plant Cell* **21**, 1733–1746 (2009).
27. M. Jeon *et al.*, Vernalization-triggered expression of the antisense transcript *COOLAIR* is mediated by *CBF* genes. *Elife* **12**, e84594 (2023).
28. Z. Zhang, X. Luo, Y. Yang, Y. He, Cold induction of nuclear FRIGIDA condensation in *Arabidopsis*. *Nature* **619**, E27–E32 (2023).
29. P. Zhu, C. Dean, Reply to: Cold induction of nuclear FRIGIDA condensation in *Arabidopsis*. *Nature* **619**, E33–E37 (2023).
30. Q. Sun, T. Csorba, K. Skourti-Stathaki, N. J. Proudfoot, C. Dean, R-loop stabilization represses antisense transcription at the *Arabidopsis FLC* locus. *Science* **340**, 619–621 (2013).
31. K. Maruyama *et al.*, Identification of cold-inducible downstream genes of the *Arabidopsis* DREB1A/CBF3 transcriptional factor using two microarray systems. *Plant J.* **38**, 982–993 (2004).
32. Y. Song *et al.*, The direct targets of CBFs: In cold stress response and beyond. *J. Integr. Plant Biol.* **63**, 1874–1887 (2021).
33. A. Abe *et al.*, Genome sequencing reveals agronomically important loci in rice using MutMap. *Nat. Biotechnol.* **30**, 174–178 (2012).
34. T. Chung, D. Wang, C. S. Kim, R. Yadegari, B. A. Larkins, Plant SMU-1 and SMU-2 homologues regulate pre-mRNA splicing and multiple aspects of development. *Plant Physiol.* **151**, 1498–1512 (2009).
35. K. Bertram *et al.*, Cryo-EM structure of a pre-catalytic human spliceosome primed for activation. *Cell* **170**, 701–713.e11 (2017).
36. S. Keiper *et al.*, Smu1 and RED are required for activation of spliceosomal B complexes assembled on short introns. *Nat. Commun.* **10**, 3639 (2019).
37. U. Ashraf *et al.*, Destabilization of the human RED–SMU1 splicing complex as a basis for host-directed antiinfluenza strategy. *Proc. Natl. Acad. Sci. U.S.A.* **116**, 10968–10977 (2019).
38. A. K. C. Ulrich, J. F. Schulz, A. Kamprad, T. Schutze, M. C. Wahl, Structural basis for the functional coupling of the alternative splicing factors Smu1 and RED. *Structure* **24**, 762–773 (2016).
39. H. Yang, M. Howard, C. Dean, Antagonistic roles for H3K36me3 and H3K27me3 in the cold-induced epigenetic switch at *Arabidopsis FLC*. *Curr. Biol.* **24**, 1793–1797 (2014).
40. F. X. Chen *et al.*, PAF1, a molecular regulator of promoter-proximal pausing by RNA polymerase II. *Cell* **162**, 1003–1015 (2015).
41. Z. Wang *et al.*, Coordinated regulation of RNA polymerase II pausing and elongation progression by PAF1. *Sci. Adv.* **8**, eabm5504 (2022).
42. A. H. Ehrensberger, G. P. Kelly, J. Q. Svejstrup, Mechanistic interpretation of promoter-proximal peaks and RNAPII density maps. *Cell* **154**, 713–715 (2013).
43. Y. He, M. R. Doyle, R. M. Amasino, PAF1-complex-mediated histone methylation of *FLOWERING LOCUS C* chromatin is required for the vernalization-responsive, winter-annual habit in *Arabidopsis*. *Genes Dev.* **18**, 2774–2784 (2004).
44. S. Oh, H. Zhang, P. Ludwig, S. van Nocker, A mechanism related to the yeast transcriptional regulator Paf1c is required for expression of the *Arabidopsis FLC/MAF* MADS box gene family. *Plant Cell* **16**, 2940–2953 (2004).
45. Y. Cao, L. Wen, Z. Wang, L. Ma, SKIP interacts with the Paf1 complex to regulate flowering via the activation of *FLC* transcription in *Arabidopsis*. *Mol. Plant* **8**, 1816–1819 (2015).
46. X. Fang *et al.*, *Arabidopsis* FLL2 promotes liquid–liquid phase separation of polyadenylation complexes. *Nature* **569**, 265–269 (2019).
47. E. Mateo-Bonmatí *et al.*, A CPF-like phosphatase module links transcription termination to chromatin silencing. *Mol. Cell* **20**, 2272–2286 (2024).
48. G. Menon *et al.*, Proximal termination generates a transcriptional state that determines the rate of establishment of Polycomb silencing. *Mol. Cell* **20**, 2255–2271 (2024).
49. F. M. Schomburg, D. A. Patton, D. W. Meinke, R. M. Amasino, *FPA*, a gene involved in floral induction in *Arabidopsis*, encodes a protein containing RNA-recognition motifs. *Plant Cell* **13**, 1427–1436 (2001).
50. S. Naftelberg, I. E. Schor, G. Ast, A. R. Kornblihtt, Regulation of alternative splicing through coupling with transcription and chromatin structure. *Annu. Rev. Biochem.* **84**, 165–198 (2015).
51. Z. Wu *et al.*, Quantitative regulation of *FLC* via coordinated transcriptional initiation and elongation. *Proc. Natl. Acad. Sci. U.S.A.* **113**, 218–223 (2016).
52. P. Singh, E. P. Ahi, The importance of alternative splicing in adaptive evolution. *Mol. Ecol.* **31**, 1928–1938 (2022).
53. P. Cui, L. Xiong, Environmental stress and pre-mRNA splicing. *Mol. Plant* **8**, 1302–1303 (2015).
54. I. Jabre *et al.*, Does co-transcriptional regulation of alternative splicing mediate plant stress responses? *Nucleic Acids Res.* **47**, 2716–2726 (2019).
55. E. Petrillo *et al.*, A chloroplast retrograde signal regulates nuclear alternative splicing. *Science* **344**, 427–430 (2014).
56. K. Sugaya, E. Hongo, H. Tsuji, A temperature-sensitive mutation in the WD repeat-containing protein Smu1 is related to maintenance of chromosome integrity. *Exp. Cell Res.* **306**, 242–251 (2005).
57. K. Sugaya, E. Hongo, Y. Ishihara, H. Tsuji, The conserved role of Smu1 in splicing is characterized in its mammalian temperature-sensitive mutant. *J. Cell Sci.* **119**, 4944–4951 (2006).
58. H. Yang, MutMap of mrcc1. China National Center for Bioinformation. https://download.cncb.ac.cn/gsa2/CRA013281. Deposited 26 October 2024.